Sigma J Eng & Nat Sci 38 (3), 2020, 1073-1098

Sigma Journal of Engineering and Natural Sciences
Sigma Mühendislik ve Fen Bilimleri Dergisi

Research Article

RELATIONAL DESCRIPTION OF AN ADSORPTION SYSTEM BASED ON ISOTHERM, ADSORPTION DENSITY, ADSORPTION POTENTIAL, HOPPING NUMBER AND SURFACE COVERAGE

Chukwunonso O. ANIAGOR*[1], Matthew Chukwudi MENKITI[2]

[1]*Chemical Eng. Department, Nnamdi Azikiwe University, Awka, NIGERIA;* ORCID: 0000-0001-6488-3998
[2]*Chemical Eng. Department, Nnamdi Azikiwe University, Awka, NIGERIA;* ORCID: 0000-0001-8552-3756

Received: 26.11.2019 Revised: 16.01.2020 Accepted: 16.01.2020

ABSTRACT

Gossweilerdendron balsamiferum (Tola wood) dust, as a precursor was used for the production of acid-activated carbon (TDAC) employed in the adsorptive removal of Cu^{2+} and Pb^{2+} ions. The relational adsorptive behaviour of TDAC, equilibrium studies and statistical evaluation of the data prediction performance of the respective models were conducted. The adsorbent was characterized using scanning electron microscopy (SEM) and Fourier transform infrared spectroscopy. Removal efficiencies of 75.66 % (for Cu-loaded TDAC) and 72.22 % (for Pb-loaded TDAC) were recorded at optimum pH (pH 6.0). The values of adsorption density, adsorption potential, hopping number and surface coverage were 7.256E-13 mol/L; -4920.78 J/mol; 8.44; 0.86 and 9.623E-13 mol/L; -5648.6 J/mol; 8.53; 0.86, for Cu- and Pb-loaded TDAC, respectively. Modified Langmuir model emerged as the best fit model for both adsorption system, as it depicted the lowest average error values of 1.8E-11 (for Cu-loaded TDAC) and 1.43E-12 (for Pb-loaded TDAC). Furthermore, model prediction performance showed that 5-parameter equation with *t-* and p-*values* of -0.862; 0.439 (for Cu-loaded TDAC) and -0.804; 0.466 (for Pb-loaded TDAC), was the least predictive among the isotherm models. The study demonstrated the effective application of TDAC in Cu^{2+} and Pb^{2+} adsorption, with the Cu-loaded TDAC being more efficient.
Keywords: Adsorption, heavy metal, isotherm, adsorption density, adsorption potential, activated carbon.

1. INTRODUCTION

The existence of unwholesome water occasioned by the incessant contamination of important water sources constitute a major challenge to water resource users; as well as threatens the ecosystem [1]. Roger, [2] predicted that about 4 – 5 billion of the world's population will experience severe clean water shortage by 2025 if the water pollution issues are not conscientiously addressed. Heavy metals are major clean water pollutants consisting of elements with atomic densities greater than 6 g/cm^3; hence, they are highly toxic to humans and other living species. These elements are usually discharged into water bodies through effluent from several process industries (such as textile, mining, paper, plastics, et.c) [3]. Meanwhile, the toxicity of the element depends on the nature of the heavy metal and an individuals' degree of exposure [3]. In this study, copper (Cu^{2+}) and lead (Pb^{2+}) ions are the heavy metal of focus.

* Corresponding Author: e-mail: aniagor@yahoo.com, tel: +234 -8061232153

Due to the cardinali ty of clean water to human existence, there is a need to ensure that industrial wastewaters meet the permissible/safe effluent discharge standards [4]. To satisfy this need, a variety of treatment techniques has been explored for the remediation of heavy metal-laden effluent. Coagulation/flocculation [5 – 6], chemical oxidation [7], ozonation [8], ion exchange [9], solvent extraction [10], photocatalytic degradation [11] and adsorption [12 – 13] rank among the best treatment options. However, the adsorption treatment technique is preferred to other techniques due to the ease and flexibility of its operation, its non-sophisticated equipment requirements and the adsorbent reusability. Activated carbon, a versatile adsorbent exhibits high adsorption capacity due to its porous structure and extended surface area; thus making it the most adopted adsorbent [14 – 15]. However, the high cost of commercially available activated carbon has fueled the drive towards developing alternative and efficient low-cost activated carbon.

Sawdust or wood dust, a by-product of cutting, grinding or drilling of wood using saw is composed of fine wood particulates. Despite its (sawdust) application in wood pulp, mulch and as fuel; it could portend serious environmental and health hazards. For instance, wood dust when inhaled (by humans and animals) could trigger severe allergic reactions; as some wood dust contain inherent toxins [16]. Similarly, accumulation of sawdust on landfills sequel to large scale wood processing could introduce harmful components domicile in the wood (such as lignins and fatty acids) as leachates into the nearby aquatic environment. The accumulation of such toxins could be detrimental to the survival of a broad range of organisms [17]. Therefore, the successful conversion of these wood dust to low cost activated carbon and their subsequent adoption as an effective replacement for the commercially available activated carbons would significantly limit the incidences of environmental pollution associated with their (sawdust) indiscriminate discharge. In this current isothermic study, TDAC was synthesized and its probable application in Cu^{2+} and Pb^{2+} ion adsorption was explored. To ensure large scope analyses of the obtained isothermic experimental data, this work relationally investigated the adsorption density, adsorption potential, hopping number and adsorbents surface coverage of the system. It also evaluated the fitting ability of 29 nonlinear isotherm models (comprising of 1-parameter, 2-parameter, 3-parameter, 4-parameter and 5-parameter models) using 5 goodness-of-fit test models (Go-FM) (Table 1).

Go-FM test, as the name implies is widely applied for measuring and testing how well respective modelled/predicted data correspond with the observed (experimental) data. In a goodness-of-fit test, the goodness of a given nonlinear isotherm model fit is solely dependent on how "closely enough" the models' assumption(s) hold for a given adsorption system; since nonlinear models are usually valid over given set of assumptions. However, the ineffective quantitative definition of 'how close enough' the respective models' assumptions are obeyed in an adsorption system remains a major drawback in the use of the Go-FM test. Although, it is commonly assumed that "the smaller the Go-FM error value, the better the model fit"; however, this assertion does not provide an operational value or models' data prediction efficiency. Thus, the present study aims at circumventing the GO-FM test limitation by further quantifying (using Statistical Package for Social Science, SPSS software version 13.0) the overall adsorption capacity ($q_{e,\,cal}$) predictive performance of the respective isotherm models (grouped based on their number of parameters). Such analyses will also provide useful insight as to how the number of parameters of a given nonlinear model could influence the quality of its data modelling and prediction.

The purpose of the work is concisely captured as follows: (1) to synthesize acid activated carbon from Tola (wood) dust (TDAC). (2) to characterize the prepared TDAC using FTIR and SEM. (3) to investigate the adsorption density/potential and the effect of solution pH on the adsorption process (4) to conduct the equilibrium studies regarding the present adsorption system. (5) to statistically evaluate the nonlinear isotherm models' adsorption capacity ($q_{e,\,cal}$) prediction performance.

2. MATERIAL AN D METHODS

2.1. Materials

Tola wood dust was collected from a wood sawmill located in the Umuokpu timber market located along Enugu-Onitsha Expressway, Awka, Anambra State, Nigeria. Copper sulfate ($CuSO_4.5H_2O$), Lead nitrate ($Pb(NO_3)_2$), as well as all other chemicals utilized in the study were all of the analytical reagent grades and purchased from the chemical market at Onitsha, Anambra state.

2.2. Preparation of Tola dust activated carbon (TDAC)

After collection, inherent dirt was eliminated from the Tola wood dust (TWD) via washing with distilled water. This was preceded by sundried and oven drying at 80 ^oC unto constant dried weight. A specific quantity of the dried TWD sample was further charged into a muffle furnace and carbonized at 450 ^oC for 50 min, followed by cooling in a desiccator.

Tola dust activated carbon was prepared by direct impregnation method as reported by Larous and Meniai, [18] with few changes. The relevant modification to this procedure is stated herein: a specific amount of charred/carbonized TWD was impregnated in 40 % w/w ortho-phosphoric acid. The temperature of the mixture was maintained at 80 ^oC for 2 h using a magnetic stirrer hot plate fitted with a thermostat. Afterwards, the activated carbon (desired) was obtained from the resultant dark slurry as residue via filtration using muslin sack. The obtained activated carbon (residue) was washed with distilled water and soaked in 1 % w/w sodium bicarbonate solution overnight to remove any residual acid. It was then washed with distilled water until pH 7.0; oven-dried at 80 ^0C until constant dry weight and stored in an airtight container, ready for use.

2.3. Batch adsorption studies and analytical method

The simulated effluent stock solution was prepared by dissolving 0.3 g of Copper sulfate ($CuSO_4.5H_2O$) or Lead nitrate ($Pb(NO_3)_2$), as the case may be, in 1 L of distilled water. Batch adsorption study was conducted by agitating (using a magnetic stirrer at 50 rpm) 1.0 g of Tola dust activated carbon, TDAC [19], with 100 mL simulated effluent of varying concentrations (50, 75, 100, 125 and 150 mg/L). Each concentration batch was placed in a given conical flask. The experiment proceeded at 30 ^oC and constant pH for 2 h to foreclose any doubt regarding the attainment of equilibrium. The equilibrium concentration values obtained for the various concentration ranges studied were employed for the equilibrium isotherm studies. Meanwhile, an equilibrium/optimum contact time of 30 min was established in the study.

To investigate the effect of solution pH on adsorption efficiency, TDAC dosage of 1.0 g each were contacted (in the respective conical flask) with the effluent of constant volume, temperature and concentration of 100 mL, 30 ^0C and 50 mg /L, respectively at various pH (3.0, 4.0, 5.0, 6.0, 7.0 and 8.0). Test samples were withdrawn from each set – up at 5 min time interval, until the consummation of the optimum contact time. Digital pH meter (HACH® India) was utilized in solution pH measurement, while 1.0 N NaOH and 1.0 N HCl solutions were used in adjusting the initial pH of the solution. To curb the introduction of uncertainty in result analysis (as a result of interference of small suspended adsorbent particles during instrumental analysis), all the collected test samples were filtered using 0.45 μm filter papers. The respective effluent concentrations (before and after adsorption) were determined using an atomic absorption AA spectrophotometer (RAYLEIGH) operating with an air-acetylene flame. The amounts of metal ions adsorbed at equilibrium, qe (mg/g) was calculated by Eq. 1;

$$q_e = \frac{(C_o - C_e)V}{W} \quad (1)$$

Where; C_e (mg/L) is the equilibrium metal ion concentration.
C_o (mg/L) is the initial metal ion concentration.
V (mL) is the effluent volume.
W (g) is the mass of adsorbent.

The number of adsorbate molecules adsorbed in terms of percentage was calculated via Eq**. 2;**

$$RE(\%) = \frac{Co-Ce}{Co} \times 100 \quad (2)$$

Insight into the adsorption behaviour of Cu^{2+} and Pb^{2+} ions could be obtained by estimating their molecular packing on the adsorbents' surface and the probability of identifying a vacant site on the adsorbent. The estimation regarding the adsorbates molecular packing was executed via thermodynamic consideration of the adsorption potential (A) and adsorption density (Γ) at constant temperature and initial concentration of 30 ^oC and 50 mg/L, respectively. Adsorption potential and adsorption density are evaluated from Eqns. 3 – 4 [20 – 21];

$$A = -RTln\left(\frac{C_o}{C_e}\right) \quad (3)$$

$$\Gamma = ZrC_e exp - \left(\frac{\Delta G^0{}_{ads}}{R}\right) \quad (4)$$

Where; C_o and C_e are the initial and equilibrium adsorbate concentration (mol/L), Γ is adsorption density (mol/L), Z is the valency of the respective heavy metals (adsorbate), r is the ionic radius of the adsorbate (meter), R is the gas constant ($J{\cdot}K^{-1}{\cdot}mol^{-1}$) and T is the absolute temperature (K). Similarly, the probability of identifying potential vacant sites for adsorption correlates to the number of hopping performed by the adsorbate molecules before sticking to a given vacant site.

The relationship between hopping number and adsorbent surface coverage is expressed as Eq. 5 [20 – 21];

$$n = \frac{1}{(1-\theta)\theta} \quad (5)$$

Where surface coverage is given by Eq. 6;

$$\theta = \left(1 - \frac{C_e}{C_o}\right) \quad (6)$$

Where; n = hopping number, $\boldsymbol{\theta}$ = surface coverage.

2.4. Brief description of the studied isotherm and goodness-of-fit models

Isotherm models are mostly adopted for effective description (via curve fittings) of the phenomenon involved in solute transport from the bulk solution to a porous solid phase (at given experimental conditions). Such a description is usually achieved by establishing a mathematical correlation between the experimental data and the predicted data. Over time, a wide range of isotherm and Go-FM models have been formulated and applied for effective adsorption modelling. The theoretical background and assumptions regarding these models are stated thus;

Henry model is a linear equation that serves an effective link between the bulk fluid and the adsorbed phase at equilibrium concentration. The model is suitable for fitting solute adsorption onto a uniform adsorbent surface, especially at low adsorbate concentration. Langmuir model has been popularly used for the study of solid-liquid phase adsorption by many authors irrespective of the fact that it was primarily designed for gas-solid phase adsorption system. However, the role of solution concentration on the desorption rate for a solid-liquid phase adsorption system is often unclear. Therefore, the modified Langmuir isotherm helps to eliminate the obvious uncertainty regarding the influence of solute concentration on the desorption rate in a solid-liquid phase adsorption system. Freundlich, Jovanovich, Halsey and Harkins-Jura isotherm are common 2-parameter empirical models, most of which are only valid for low or high ion concentration; thus limiting their versatility and applicability. Redlich-Peterson, Sip, Toth, Brouer-Sotolongo, Koble-

Corrigan, Khan, Fritz-Schlunder III and Radke-Prausnitz models are all 3-parameter isotherms, originating from an effective combination of Langmuir and Freundlich model characteristics; thereby circumventing the prediction error associated with the use of single model characteristics. Aforementioned 3 – parameter models, as well as Vieth-Sladek, Jossen, Holl-Krich and Unilan models, are readily applied in the description of adsorption onto heterogeneous surfaces. Hill isotherm model describes the binding of an adsorbate species onto the homogeneous adsorbent surface. Tempkin isotherm assumes a uniform binding energy distribution and also considers the possible influence of adsorbate interaction on a given adsorption system. Langmuir-Freundlich-Jovanovich (L-F-J) model is useful in the analysis and evaluation of probable mechanism, adsorbent-adsorbate affinity and maximum adsorption capacity in a given adsorption system. Modified Langmuir-Freundlich (M-L-F), Jovanovich-Freundlich (J-F) and Langmuir-Jovanovich (L-F) models are all empirical. They do not follow the postulations of Henry's law but are effective in elucidating the differential relationship between surface coverage and bulk concentration. Marczewski–Jaroniec, Baudu, Fritz–Schlunder–IV and Fritz–Schlunder–V isotherm models are also empirical models but with an increased number of parameters. They could reduce to either Langmuir or Freundlich depending on the respective parametric values and could be employed effectively over expanded equilibrium data.

The coefficient of determination (R^2) describes the degree to which specified input variables elucidate the divergence in the output / predicted variables. Numerically larger R^2-value implies a better explanation for the variability in the output variable by the input variables. However, the major limitation of R^2 is its tendency to either remain constant or increase with an increase in the number of respective model parameters, irrespective of their influence on the output variables. Adjusted R^2 (R^2_{adj}) also explains the variation in the output variable regarding the input variables. Besides, it (R^2_{adj}) considers the number of parameters in a model and how the parameter addition will improve the models' data prediction accuracy. Hybrid fractional error function (HYBRID) offer an improved version of the sum of squared error (ERRSQ) by putting into consideration the number of parameters in the isotherm equation. Reduced chi-square (X^2) test is used to ascertain the best fit model for an adsorption system by evaluating the sum of the squared difference between the input variables and the corresponding output variables. As a measure of accuracy, root mean squared error (RMSE) compares the predicted errors obtained for different models to a given experimental dataset. It also represents the square root of the differences between output/predicted variables and input/experimental variables. The Go-FM and isotherm models employed in this study are listed in Tables 1 and 2, respectively.

Table 1. Equations of applied error functions

Error Function	Expression	References	Eq. no
R^2	$\frac{(q_{e,exp} - \overline{q_{e,Calc}})2}{\sum(q_{e,exp} - \overline{q_{e,Calc}})2 + (q_{e,exp} - q_{e,Calc})2}$	[22]	(7)
Adjusted R^2	$1 - \frac{\sum_{i=1}^{n}(q_{e,calc.} - q_{e,exp})^2 / n-p}{\sum_{i=1}^{n}(q_{e,exp} - \overline{q_{e,exp}})^2 / n-1}$	[22]	(8)
Reduced X^2	$\frac{1}{(n-p)}\sum_{i=1}^{n}(q_{e,calc.} - q_{e,exp})^2$	[23]	(9)
HYBRID	$\frac{100}{n-p}\sum\left[\frac{(q_{e,exp} - q_{e,Calc})2}{q_{e,exp}}\right]$	[24]	(10)
RMSE	$\sqrt{\frac{1}{(n-p)}\sum_{i=1}^{n}(q_{e,calc.} - q_{e,exp})^2}$	[25]	(11)

Table 2. List of studied Isotherm models

Isotherm models	Nonlinear form	Remarks	References	Eq. no.
Henry's Law	$q_e = K_H C_e$	1- parameter model	**[26]**	(12)
Modified Langmuir	$q_e = \frac{q_M K_{ML} C_e}{(C_s - C_e) + K_{ML} C_e}$	2-parameter model	**[27]**	(13)
Freundlich	$q_e = K_F (C_e)^{\frac{1}{n_F}}$	2-parameter model	**[28]**	(14)
Tempkin	$q_e = \frac{RT}{b_T} ln(K_T C_e)$	2-parameter model	**[29]**	(15)
Halsey	$q_e = exp\left(\frac{lnK_{Ha} - lnC_e}{n_{Ha}}\right)$	2-parameter model	**[30]**	(16)
Harkins-Jura	$q_e = \sqrt{\frac{A_H}{B_H + \log C_e}}$	2-parameter model	**[30]**	(17)
Jovanovich	$q_e = q_{mJ}\left[1 - exp(-K_J c_e)\right]$	2-parameter model	**[31]**	(18)
Redlich-Peterson	$q_e = \frac{K_{RP} C_e}{1 + \alpha_{RP} (C_e)^{\beta}}$	3-parameter model	**[32]**	(19)
Sips	$q_e = \frac{K_S q_{mS} (C_e)^{\frac{1}{m_S}}}{1 + K_S (C_e)^{\frac{1}{m_S}}}$	3-parameter model	**[33]**	(20)
Toth	$q_e = \frac{q_{mT} K_T C_e}{[1 + (K_T C_e)^{n_T}]^{\frac{1}{n_T}}}$	3-parameter model	**[34]**	(21)
Brouers-Sotolongo	$q_e = q_{mBS}[1 - exp(-K_{BS}(C_e)^{\alpha})]$	3-parameter model	**[35]**	(22)
Vieth-Sladek	$q_e = K_{VS} C_e + \frac{q_{mVS} \beta_{VS} C_e}{1 + \beta_{VS} C_e}$	3-parameter model	**[36]**	(23)
Koble-Corrigan	$q_e = \frac{A_{KC} B_{KC} {C_e}^{n_{KC}}}{1 + B_{KC} {C_e}^{n_{KC}}}$	3-parameter model	**[37]**	(24)
Khan	$q_e = \frac{q_{mK} b_K C_e}{(1 + b_K C_e)^{a_K}}$	3-parameter model	**[38]**	(25)
Hill	$q_e = \frac{q_{mH} {C_e}^{n_H}}{K_H + {C_e}^{n_H}}$	3-parameter model	**[39]**	(26)
Jossens	$q_e = \frac{K_J C_e}{1 + a_J {C_e}^{b_j}}$	3-parameter model	**[40]**	(27)

Continued from **Table 2**

Isotherm models	Nonlinear form		Reference	Eq. no.
Fritz-Schlunder-III	$q_e = \frac{q_{mFS} K_{FS} C_e}{1 + K_{FS} {C_e}^{n_{FS}}}$	3-parameter model	**[41]**	(28)
Unilan	$q_e = \frac{q_{mU}}{2s} \ln\left[\frac{1 + K_U C_e exp(s)}{1 + K_U C_e exp(-s)}\right]$	3-parameter model	**[40]**	(29)
Holl-Krich	$q_e = \frac{q_{mHK} K_{HK} {C_e}^{n_{HK}}}{1 + K_{HK} {C_e}^{n_{HK}}}$	3-parameter model	**[38]**	(30)

Modified Langmuir-Freundlich	$q_e = \frac{(K_{mLF}C_e)^{n_{mLF}}}{(C_s - C_e)^{n_{mLF}} + (K_{LF}C_e)^{n_{mLF}}}$	2-parameter model	**[27]**	(31)
Langmuir-Jovanovich	$q_e = \frac{q_{mLJ}C_e\left[1 - exp\left(K_{LJ}{C_e}^{n_{LJ}}\right)\right]}{1 + C_e}$	3-parameter model	**[42]**	(32)
Jovanovich-Freundlich	$q_e = q_{mJF}\left[1 - exp\left(-K_{JF}C_e\right)^{n_{JF}}\right]$	3-parameter model	**[43]**	(33)
Radke–Prausnitz – I	$q_e = \frac{q_{mR}K_RC_e}{(1 + K_RC_e)^{m_R}}$	3-parameter model	**[40]**	(34)
Radke–Prausnitz – II	$q_e = \frac{q_{mR}K_RC_e}{1 + K_R{C_e}^{m_R}}$	3-parameter model	**[40]**	(35)
L-F-J	$q_e = \frac{q_{mLFJ}{C_e}^{n_{LFJ}}\left[1 - exp\left(-\left(K_{LFJ}C_e\right)\right)^{n_{LFJ}}\right]}{1 + {C_e}^{n_{LFJ}}}$	3-parameter model	**[44]**	(36)
Marczewki-Jaroniec	$q_e = q_{mMJ}\left[\frac{\left(K_{MJ}C_e\right)^{n_{MJ}}}{1 + \left(K_{MJ}C_e\right)^{n_{MJ}}}\right]^{\frac{m_{MJ}}{n_{MJ}}}$	4-parameter model	**[44]**	(37)
Baudu	$q_e = \frac{q_{mB}b_BC_e^{(1+x+y)}}{1 + b_BC_e}$	4-parameter model	[**45]**	(38)
Fritz-Schlunder-IV	$q_e = \frac{A_{FS}{C_e}^{a_{FS}}}{1 + B_{FS}{C_e}^{b_{FS}}}$	4-parameter model	**[41]**	(39)
Fritz-Schlunder-V	$q_e = \frac{q_{mFS5}K_1{C_e}^{\alpha_{FS5}}}{1 + K_2{C_e}^{\beta_{FS5}}}$	5-parameter model	**[41]**	(40)

- L-F-J is Langmuir-Freundlich-Jovanovich model

3. RESULT AND DISCUSSIONS

3.1. Surface chemistry

Generally, the presence of functional groups on an adsorbent determines their adsorption capacity. The study of the pre-and post-adsorption surface chemistry of TDAC using Fourier transform infrared spectroscopy (FTIR) was conducted to investigate the probable functional groups culpable for the adsorption process. Fig 1 and Table 3 presented, respectively the FTIR spectra and probable functional groups existing on the unloaded and metal-loaded TDAC. Usually, – OH and – NH groups (important functional groups in organic materials) could both exist at wave number around 3400 cm^{-1}. Both functional groups can only be differentiated by the shape of their respective peaks at the said wave number. For unloaded-TDAC, this important functional group (– OH and – NH) was observed on 3413.15 cm^{-1} band and it subsequently shifted to 3421.16 cm^{-1} (for Cu-loaded TDAC) and 3431.54 cm^{-1} (for Pb-loaded TDAC) after adsorption. Considering the broad shape of the peak, the occurrence of the O-H absorption band of carboxylic acid (O=C–OH) rather than the comparatively narrower N-H bond and O-H absorption band of alcohol or C–OH (which also exist at the similar band) is most likely. Aliphatic C – H asymmetric stretching is another vital functional group that ensured efficient adsorption as the wave number which originally appeared at 2919.50 cm^{-1} (for unloaded TDAC) shifted to 2926.36 cm^{-1} (for Cu-loaded TDAC) and 2930.44 cm^{-1} (for Pb-loaded TDAC). The involvement of the C≡C stretching band in the adsorption process cannot be overlooked, as its wave number representation (2364.31 cm^{-1}, for unloaded TDAC) shifted to 2361.73 cm^{-1} (for Cu-loaded TDAC) and 2343.74 cm^{-1}(for Pb-loaded TDAC). Furthermore, the appearance of peaks in the unloaded TDAC around 1696.74 cm^{-1} (C = O stretching bond) and 1541.11 cm^{-1} (secondary amide N–H bending), which shifted consequent upon Cu^{2+} and Pb^{2+} ion adsorption (as shown in

Table 3) is indicative of their respective involvement in the heavy metal uptake. The observable peaks at 1717.92 and 1734.37 cm^{-1} (Table 3) for Cu-loaded and Pb-loaded TDAC, respectively (which was absent in the unloaded TDAC) indicate the presence of adsorbed heavy metal (Cu^{2+} and Pb^{2+}) on the respective adsorbents. Also notable in Table 3 was the occurrence of an aliphatic phosphate stretching band on 1038.78 cm^{-1} (for unloaded TDAC). However, the aliphatic phosphate stretching band shifted slightly to 1042.72cm^{-1} (for Cu-loaded TDAC) and 1042.99 cm^{-1} (for Pb-loaded TDAC) sequel to adsorption.

From the adsorbent surface chemistry, it is clear that the pre and post adsorption FTIR spectra of the respective metal loaded TDAC (Cu-loaded TDAC and Pb-loaded TDAC) in comparison with the unloaded TDAC showed an obvious shift in some represented wavenumbers (Fig 1 and Table 3). Such wave number shifts could be due to the attachment of the respective metal ions [Pb^{2+} and Cu^{2+}] onto the adsorbents' surface either by ionic complexation, weak electrostatic interaction or Van der Waal forces. It could also be due to the formation of new complexes at the adsorbents' active sites due to the likely release of the proton from the carboxyl and hydroxyl groups present on TDAC surface.

Table 3. Dominant peaks on the adsorbent and their assigned function groups

Functional groups	Unloaded TDAC (cm^{-1})	Cu-loaded TDAC (cm^{-1})	Pb-loaded TDAC (cm^{-1})
Hydroxyl group, H-bonded OH stretch	3413.15	3421. 16	3431.54
Methyl C-H asymmetric stretch	2919.50	2926.36	2930.44
C≡C stretching band	2364.31	2361.73	2343.74
Unsaturated Carbonyl stretching, C= O bond	1696.74	1636.40	1684.43
Secondary amide N–H bending, C–N stretching	1541.11	1540.76	1521.85
Metal carbonyl group	X	1717.92	1734.37
Aliphatic phosphates (P-O-C stretch)	1038.78	1042.72	1042.99

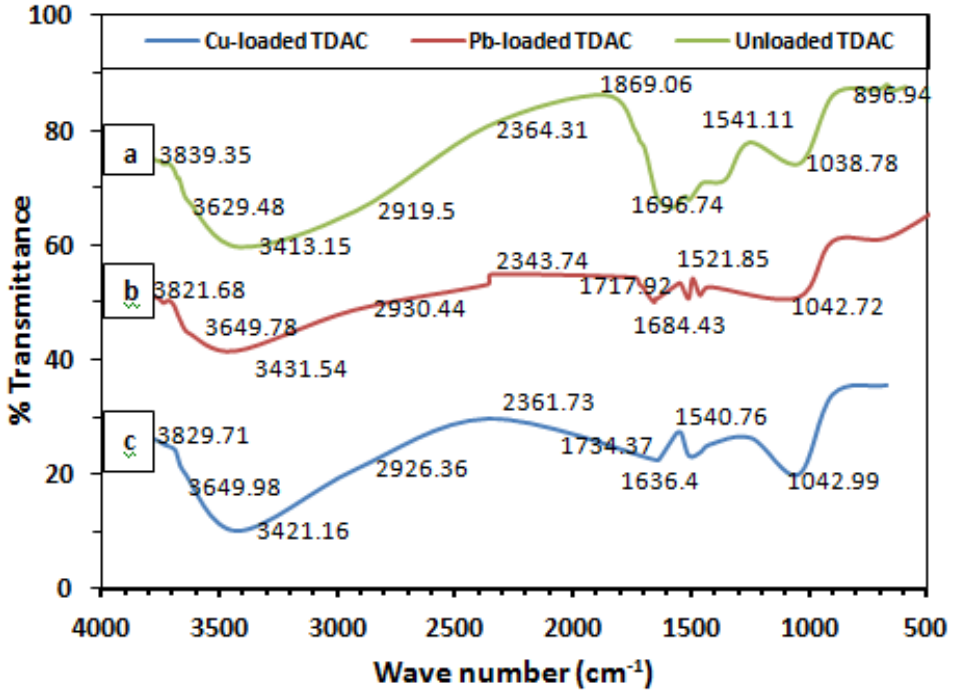

Figure 1. FTIR spectra for (a) Unloaded (b) Pb-loaded (c) Cu-loaded TDAC

3.2.Surface morphology

The surface morphologies of Tola sawdust (TD) and Tola dust activated carbon (TDAC) as shown in Fig. 2, were both slightly rough and uneven. TDAC surface is more rough and uneven; thus depicting a more significant pore structure when compared to those of TD. The pore development in TDAC is due to the breakdown of the inherent lignocellulosic material of TD sequel to carbonization. More so, the action of the acid activation agent (H_2PO_3) during activation could have resulted in high carbon burn off; a viable catalyst for improved TDAC porosity [46]. In addition to the increased TDAC porosity, the carbon – H_2PO_3 reaction could also create new pores/adsorption sites due to the potential loss of volatile components in the forms of CO and CO_2 [46]. Thus, the physicochemical activation step translates effectively to an improved adsorbent porosity with an attendant positive implication of the heavy metal ion uptake.

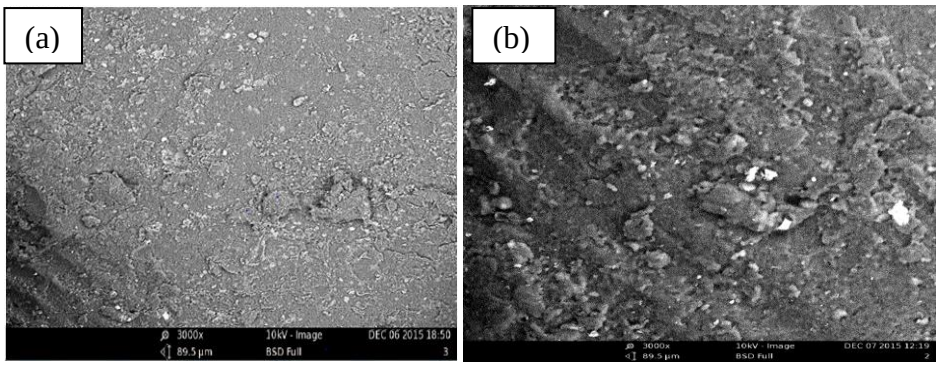

Figure 2. SEM Images for (a) unloaded TDAC (b) loaded TDAC

3.2. Effect of pH

The information regarding the optimum solution pH is vital for any adsorption system; as it affects the adsorbents' surface charge, as well as modulates the adsorbates' degree of ionization and speciation during adsorption [47]. In this study, the relationship between solution pH, adsorbate percentage removal and adsorption capacity (mg/g) was investigated in the pH range of 2.0 to 8.0 and depicted in Figs. 3 (a-b). It was however observed that the TDAC adsorption capacity and % removal was enhanced when the pH of the respective effluents appreciated. Detailed observation of Figs. 3(a-b) showed a low adsorption capacity (1.695 and 1.543 mg/g for Cu- and Pb-loaded TDAC, respectively) and percentage removal (33.894 and 30.8586 % for Cu- and Pb-loaded TDAC, respectively) in the pH range of 2.0 to 3.0 (very low pH). This could be because at this pH range, the number of available H_3O^+ ions greatly exceeded those of the metal ion (Pb^{2+} and Cu^{2+} ions); hence, they (metal ions) could hardly compete with the H_3O^+ ions for the binding sites on TDAC. Similarly, the possible protonation of the hydroxyl and carbonyl groups on the adsorbent (as shown by Eqs. 41 – 42) could further heighten the ionic competition effect. This phenomenon (ionic competition effect) must be reasonably overcome before the metal ions (M^{2+}) could adsorb onto the TDAC surface or else they would be held within the bulk liquid phase.

$$S - OH_{(s)} + H^+_{(aq)} \longrightarrow S - OH_{2\,(aq)}^+ \ (\text{protonation})[+ M^{2+}\ (\text{repulsion})] \quad (41)$$

$$S - [C = O]_{(s)} + H^+_{(aq)} \longrightarrow S - [C = OH^+]_{(aq)}\ (\text{protonation})\ [+ M^{2+}\ (\text{repulsion})] \quad (42)$$

[Where; Pb^{2+} and Cu^{2+} are denoted as M^{2+}; S denotes the adsorbent surface]

Further, increase in effluent pH from pH 3.0 to 4.0 showed an almost doubled adsorption capacity (3.04 and 2.87 mg/g for Cu- and Pb-loaded TDAC, respectively) and uptake efficiency (60.84 and 57.47 % for Cu- and Pb-loaded TDAC, respectively); a probable consequence of a considerable reduction in the H_3O^+ ions concentration. This reduction will, in turn, liberate some of the TDAC adsorption sites; thus making them available for metal ions (M^{2+}) adsorption. Interestingly, as the pH increased further from pH 4.0 through pH 5.0 to pH 6.0, a sustained increase in adsorption capacity and uptake efficiency of TDAC was observed. This could be due to further reduction in effluent acidity, thereby making it possible for the respective metal ions to effectively occupy the active sites on the TDAC surface, which were initially occupied by H_3O^+ ions. Meanwhile, the adsorption capacity (3.79 and 3.62 mg/g for Cu- and Pb-loaded TDAC, respectively) and uptake efficiency (75.78 and 72.43 mg/g for Cu- and Pb-loaded TDAC,

respectively) was virtually constant with pH increase from pH 6.0 to 7.0; followed by a disproportionately large increase in the extent of adsorption (> 95 % in both systems) with higher pH (beyond pH 7.0). The occurrence of hydrolysis and subsequent precipitation of Pb^{2+} and Cu^{2+} as insoluble hydroxide (as shown in Eqs. 43 – 44) at pH beyond pH 7.0 offers a probable explanation to the disproportionately large increase in the extent of adsorption.

$$Pb^{2+}{}_{(aq)} + 2OH^{-}{}_{(aq)} \rightarrow Pb(OH)_{2\,(s)} \quad (43)$$

$$Cu^{2+}{}_{(aq)} + 2OH^{-}{}_{(aq)} \rightarrow Cu(OH)_{2\,(s)} \quad (44)$$

According to Cerozi and Fitzsimmons [47], such precipitation may introduce uncertainties in the result analyses and thus could be responsible for the observed higher metal ion uptake within the pH range (pH 7.0 to 8.0). Therefore, it would be concluded that the adsorption of the divalent metal ions (Pb^{2+} and Cu^{2+}) onto TDAC as depicted by the stoichiometry of Eqs. 45 – 46 occurred at an optimum pH of 6.0 and supported by removal efficiencies of 75.66 % (for Cu-loaded TDAC) and 72.22 % (for Pb-loaded TDAC) shown in Fig 3.

$$S - OH_{(s)} + [M^{2+}]_{(aq)} \xrightarrow[[pH_{pzc} < pH < 6.0]]{} S - O - H \cdots M \quad (45)$$

$$S - [C = O]_{(s)} + [M^{2+}]_{(aq)} \xrightarrow[[pH_{pzc} < pH < 6.0]]{H^{+}} S \cdots C = O \cdots M \quad (46)$$

[Where; S = adsorbent surface, M = metal ion]

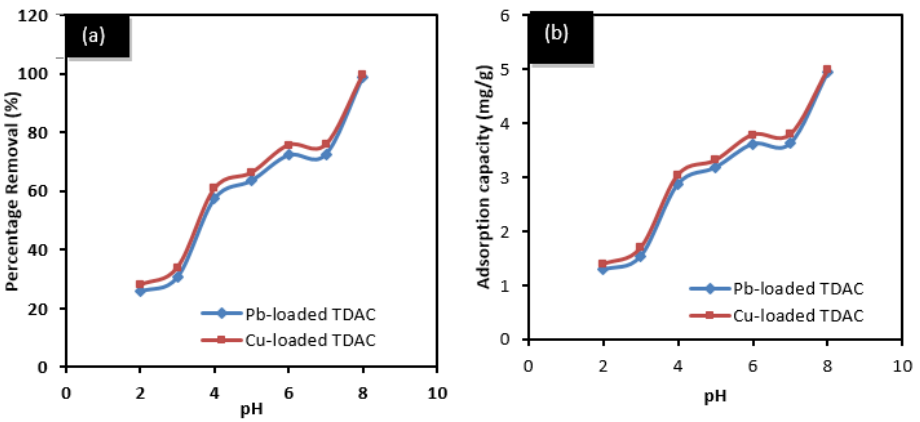

Figure 3. Plot of Influence of pH on (a) adsorption capacity (mg/g) (b) removal efficiency

3.3. Adsorption equilibrium studies

The adsorption isotherm models elucidate the movement of a given adsorbate from bulk fluid phase to adsorbent surface at a specified equilibrium state. Adsorption affinity, maximum adsorption capacity and other surface properties of the adsorbent derivable from adsorption isotherm models provide great insight into the nature of the adsorption system. Table 4 presents the isotherm and GO-FM model parameters for Cu-loaded and Pb-loaded TDAC. Remarkably, a comparison of the parametric values recorded for both adsorbent as depicted in Table 4, showed a

negligible variation of less than unity for all the models except for Sips, Toth, Brouer Sotolongo, and Vieth Sladek models; whose parametric variations are far greater than unity. Furthermore, the significance of some specified model constants concerning the present adsorption systems is summarized herein. The Freundlich isotherm, an empirical equation is useful for elucidating adsorbate-adsorbent interaction for heterogeneous systems. According to Shafique, et al. [28], the magnitude of the heterogeneity factor (n_F) is indicative of the adsorption characteristics, usually expressed as worthy/favorable ($2 < n_F < 10$), problematic ($1 < n_F < 2$) and very poor ($n_F < 1$). When $0 < \frac{1}{n_F} < 1$, adsorption is considered favourable, with increasing heterogeneity and stronger adsorbate-adsorbent interaction as the value tends to zero. Similarly, $\frac{1}{n_F} = 1$ implies linear adsorption with an attendant non-distinguishable adsorption energies for all sites [48]. The values of n_F; $\frac{1}{n_F}$ of 3.54; 0.282 (for Cu-loaded TDAC) and 2.192; 0.456 (for Pb-loaded TDAC) indicate that both processes were favorable, with decreased heterogeneity. Hence, the present system supports homogenous monolayer adsorption. Tempkin isotherm constant, b_T elucidates the nature of an adsorption process regarding heat energy distribution. A positive and negative b_T value suggests the exothermic and endothermic nature, respectively of the system. The positive b_T value of 462.92 recorded for both adsorption systems under consideration indicates the likelihood of an exothermic process. Redlich Peterson could be applied successfully in homogeneous or heterogeneous systems, depending on the magnitude of the exponent, β_{RP} [49]. When β_{RP} is equal to 1 and 0, Redlich Peterson isotherm approaches Langmuir and Freundlich isotherm, respectively. The β_{RP}-value of 0.53 and 0.596 recorded for Cu-loaded and Pb-loaded TDAC, respectively is close to unity; thus suggesting the probable occurrence of monolayer adsorption. Koble–Corrigan model constant defines the validity or otherwise of a system. $n_{KC} \geq 1$, imply a valid adsorption system, while $n_{KC} \leq 1$ signifies the models' inefficiency in defining the experimental data, despite the results from other goodness-of-fit adjudging criteria (correlation coefficient or low error value). The n_{KC}-values of 1.75 (for Cu-loaded TDAC) and 1.85 (for Pb-loaded TDAC) attest to the validity of both adsorption systems. Hills model defines adsorbate binding onto the homogenous surface as a cooperative manifestation. According to Ringot, et al. [39], a positive cooperative adsorbate binding occurs when $n_H > 1$, non–cooperative or hyperbolic binding occur when $n_H = 1$, and negative cooperativity in binding exist when $n_H < 1$. The n_H-values of 0.560 and 0.573 recorded for Cu-loaded and Pb-loaded TDAC, respectively imply the existence of negative binding cooperativity. Therefore, the attachment of adsorbates onto the adsorbent active sites progressively limits their (active sites) affinity for other ligands; thus favouring monolayer adsorption. The Unilan model as an empirical equation supposes uniformity in adsorption energy distribution. The higher the model exponent, s, the more heterogeneous the system becomes [50]. The s-values of 0.017 (for Cu-loaded TDAC) and 0.016 (for Pb-loaded TDAC) (which are numerically small) suggest the homogeneity of both adsorption systems. Marczewski–Jaroniec isotherm is notable for its supposition of adsorption energies distribution in the active sites. Its parameters m_{MJ} and n_{MJ} describe the distribution spreading in the path of higher and lower adsorption energies, respectively. When $n_{MJ} = m_{MJ} = 1$, $n_{MJ} = m_{MJ}$ or $m_{MJ} = 1$, the model reduces to Langmuir, Langmuir–Freundlich or Toth isotherm, respectively. The fact that the $n_{MJ} = m_{MJ}$-values obtained for both adsorption systems (Table 4) is approximately equal to unity suggests that the model could reduce to Langmuir model. Therefore, monolayer adsorption onto a homogenous surface would be favoured. Fritz and Schlunder V model is useful over a wide range of equilibrium data. The value of the isotherm constants determine the validity or otherwise of the model data. However, the model is valid only in the range of $\alpha_{FS} \leq 1$ and $\beta_{FS} \leq 1$. The α_{FS} and β_{FS} values recorded in this study for both systems (Table 4) effectively approximate to unity; thus indicating the models' validity. Generally, the above consideration of the various isotherm constants' significance showed that monolayer adsorption onto a homogenous surface characterized the present adsorption systems.

Table 4 further showed that the correlation coefficient (R^2 and $\overline{R^2}$) values were unity in all models for both adsorbents. This value ($R^2 = \overline{R^2} = 1$) signifies a perfect explanation of the variability in the output responses by the input variables. Therefore, based on R^2 and $\overline{R^2}$, the provision of the perfect fit of the experimental result (by all the models) would be assumed. Consequently, due to the observed vagueness as regards the selection of the best-fit isotherm model (judging the respective correlation coefficient values), further goodness-of-fit test using reduced X^2, HYBRID and RMSE error function models would be conducted. To make for unambiguous analysis, the average of the error values obtained for the three (3) Go-FM models (as presented in Table 4) for the various isotherm models will be considered. The evaluation criterion is stated thus; the lower (to zero) the average error value for a particular isotherm model, the better the models' appropriateness in describing the experimental data. Modified Langmuir model (ML) with the lowest average error value of 1.43E-12 and 1.84E-11 for Cu-loaded and Pb-loaded TDAC, respectively provided the best and unsurpassed demonstration of the experimental result. Meanwhile, the Sips model with the largest average error values of 19.26 (for Cu-loaded TDAC) and 16.39 (for Pb-loaded TDAC) was adjudged to depict a poor fitting of the experimental data. Theoretical consideration of the best fit model (modified Langmuir model) shows that just like the classical Langmuir model, the modified Langmuir model supposes monolayer adsorption of Cu^{2+} and Pb^{2+} ions onto homogenous TDAC surface, with the occurrence of non-interaction between the adsorbate and adjacent active site. However, unlike the classical Langmuir model, ML postulates the feasibility of TDAC surface saturation by the adsorbate when the equilibrium metal ions (Cu^{2+} and Pb^{2+} ion) concentration corresponds to their saturation concentration. Furthermore, the maximum adsorption capacity (q_m) value of 10.07 mg/g recorded for ML is close to the experimental q_m value of 11.98 mg/g. Another important analytical parameter, the separation factor (R_L) is relevant for verifying the unfavorable ($R_L > 1$), linear ($R_L = 1$), favorable ($0 < R_L < 1$), or irreversible ($R_L = 0$) of a given adsorption system. The range of R_L-values (Fig 4) (3.0E-3 to 8.0E-3) obtained for the studied concentration range (50 – 150 mg/L) for both Cu-loaded and Pb-loaded TDAC, indicate the favorability of both adsorption system. Notably, the decrease in R_L with initial concentration increase (Fig 4) suggests the occurrence of favourable adsorption at a higher concentration range. Further observation of Table 4 shows that the emergence of ML as the best fit model does not imply the poor fitting ability of the rest of the models. All other models except Sips model depicted relatively low error value (which are far less than unity); thus attesting to their above-average performance in predicting the variability in the output/predicted data using input/experimental data. Importantly, the emergence of ML which postulates homogenous monolayer adsorption as the best fit model is in line with the insight obtained earlier in this section while evaluating the significance of some specified model constants to the present adsorption systems.

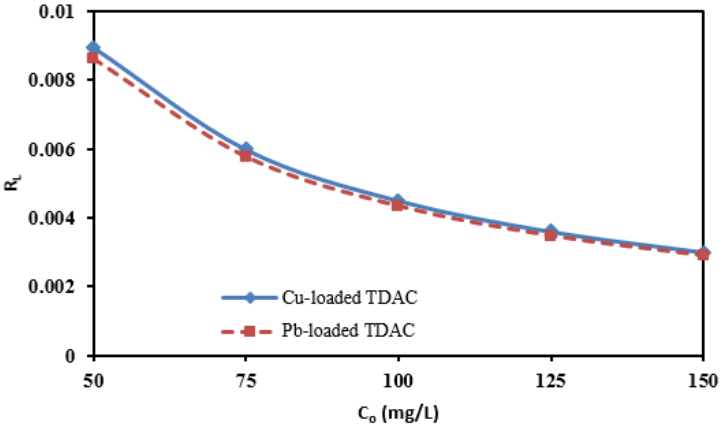

Figure 4. A plot of Langmuir separation factor (R_L)

Table 4. Isotherm parameters

Henry	Modified Langmuir	Freundlich	Tempkin	Halsey	Harkins-Jura
Cu-loaded TDAC					
K_{He} = 2.42	q_{max} = 10.07	K_F = 6.75	b_t = 462.92	K_{Ha} =14.83	A_H = 129.25
R^2 = 1	K_L = 2.21	n_F = 3.54	k_t = 1.84	n_{Ha} =2.48	B_H = 0.946
R^2_{adj} = 1	R^2 = 1	R^2 = 1	R^2 = 1	R^2 = 1	R^2 = 1
X^2 = 1.7E-17	R^2_{adj} = 1	R^2_{adj} = 1	R^2_{adj} = 1	R^2_{adj} = 1	R^2_{adj} = 1
RMSE = 4.12E-9	X^2 = 3.06E-21	X^2 = 1.26E-18	X^2 = 5.1E-13	X^2 = 9.87E-15	X^2 = 4.72E-19
HYBRID = 2.53E-17	RMSE = 5.53E-11	RMSE = 1.12E-9	RMSE = 7.12E-7	RMSE = 9.93E-8	RMSE = 6.87E-10
Average error = 1.37E-9	HYBRID = 6.36E-21	HYBRID = 2.63E-18	HYBRID = 1.1E-12	HYBRID = 2.06E-14	HYBRID = 9.83E-19
	Average error = 1.8E-11	Average error = 3.8E-10	Average error = 2.37E-7	Average error = 3.31E-8	Average error = 2.29E-10
Pb-loaded TDAC					
K_{He} = 2.518	q_{max} = 10.070	K_F = 4.359	b_t = 462.92	K_{Ha} = 14.223	A_H = 131.61
R^2 = 1	K_L = 2.294	n_F = 2.192	k_t = 1.869	n_{Ha} = 2.818	B_H = 0.954
R^2_{adj} = 1	R^2 = 1	R^2 = 1	R^2 = 1	R^2 = 1	R^2 = 1
X^2 = 4.1E-22	R^2_{adj} = 1	R^2_{adj} = 1	R^2_{adj} = 1	R^2_{adj} = 1	R^2_{adj} = 1
RMSE = 2.02E-11	X^2 = 1.845E-23	X^2 = 2.33E-17	X^2 = 1.25E-12	X^2 = 1.52E-15	X^2 = 2.43E-19
HYBRID = 8.52E-22	RMSE = 4.29E-12	RMSE = 4.8E-9	RMSE = 1.12E-6	RMSE = 3.91E-8	RMSE = 4.93E-10
Average error = 6.75E-12	HYBRID = 3.83E-23	HYBRID = 4.85E-17	HYBRID = 2.61E-12	HYBRID = 3.17E-15	HYBRID = 5.05E-19
	Average error = 1.43E-12	Average error = 1.61E-9	Average error = 3.74E-7	Average error = 1.3E-8	Average error = 1.64E-10
Jovanovich	**Redlich-Peterson**	**Sips**	**Toth**	**Brouers Sotolongo**	**Vieth Sladek**
Cu-loaded TDAC					
q_J = 9.79	K_{RP} = 69.67	q_S = 3.127	q_{To} = 6.79	q_{Bs} = 0.27	q_{Vs} = 0.858
K_J = 0.196	a_{RP} =13.152	m_S = 0.852	n_{To} = 9.62	α_{Bs} = 0.765	β_{Vs} = 13.12
R^2 = 1	β_{RP} = 0.53	k_S =10.63	k_{To} = 2.22	K_{Bs} =18.94	K_{Vs} =0.263
R^2_{adj} = 1	R^2 = 1	R^2 = 1	R^2 = 1	R^2 = 1	R^2 = 1
X^2 = 8.49E-15	R^2_{adj} = 1	R^2_{adj} = 1	R^2_{adj} = 1	R^2_{adj} = 1	R^2_{adj} = 1
RMSE = 9.21E-8	X^2 = 1.84E-16	X^2 = 2.28E-21	X^2 = 1.05E-16	X^2 = 1.26E-14	X^2 = 8.27E-17
HYBRID = 1.77E-14	RMSE = 1.36E-8	RMSE = 4.72E-11	RMSE = 1.03E-8	RMSE = 1.12E-7	RMSE = 9.1E-9
Average error = 3.1E-8	HYBRID = 3.84E-16	HYBRID = 57.77	HYBRID = 2.19E-16	HYBRID = 2.62E-14	HYBRID = 1.72E-16
	Average error = 4.53E-9	Average error = 19.26	Average error = 3.42E-9	Average error = 3.74E-8	Average error = 3.03E-9
Pb-loaded TDAC					
q_J = 9.66	K_{RP} = 69.673	q_S = 10.56	q_{To} = 9.63	q_{Bs} = 18.991	q_{Vs} = 13.131
K_J = 0.205	a_{RP} = 13.15	m_S = 0.83	n_{To} = 2.32	α_{Bs} = 0.706	β_{Vs} = 0.281
R^2 = 1	β_{RP} = 0.596	k_S = 3.126	k_{To} = 6.81	K_{Bs} = 0.299	K_{Vs} = 0.871
R^2_{adj} = 1	R^2 = 1	R^2 = 1	R^2 = 1	R^2 = 1	R^2 = 1
X^2 = 7.23E-15	R^2_{adj} = 1	R^2_{adj} = 1	R^2_{adj} = 1	R^2_{adj} = 1	R^2_{adj} = 1
RMSE = 8.5E-8	X^2 = 5.24E-16	X^2 = 6.14E-19	X^2 = 6.14E-19	X^2 = 1.43E-20	X^2 = 7.63E-20
HYBRID = 1.5E-14	RMSE = 2.29E-15	RMSE = 9.68E-11	RMSE = 7.83E-10	RMSE = 1.19E-10	RMSE = 2.76E-10
Average error = 2.84E-8	HYBRID = 1.09E-15	HYBRID = 49.13	HYBRID = 1.27E-18	HYBRID = 2.98E-20	HYBRID = 1.58E-19
	Average error = 7.63E-9	Average error = 16.39	Average error = 2.61E-10	Average error = 3.99E-11	Average error = 9.2E-11

Table 4 *continued*

Koble-Corrigan	Khan	Hills	Jossen	Fritz Schlunder III	Unilan
Cu-loaded TDAC					
A_{KC} = 10.22	q_K = 2.29	q_H = 167.23	K_{Js} = 10.44	K_{Fs} = 0.360	K_U = 3.06
B_{KC} = 4.15	a_K = 0.266	K_H = 33.81	a_{Js} = 1.75	q_{Fs} = 13.14	q_U = 8.63
n_{KC} = 1.75	b_K = 1.943	n_H = 0.56	b_{Js} = 0.423	n_{Fs} = 0.636	S_U = 0.017
R^2 = 1	R^2 = 1	R^2 = 1	R^2 = 1	R^2 = 1	R^2 = 1
R^2_{adj} = 1	R^2_{adj} = 1	R^2_{adj} = 1	R^2_{adj} = 1	R^2_{adj} = 1	R^2_{adj} = 1
X^2 = 3.18E-13	X^2 = 9.7E-15	X^2 = 9.25E-15	X^2 = 2.45E-12	X^2 = 1.01E-14	X^2 = 1.32E-13
RMSE = 5.64E-7	RMSE = 9.85E-8	RMSE = 9.62E-8	RMSE = 1.56E-6	RMSE = 1.01E-7	RMSE = 3.64E-7
HYBRID = 6.62E-13	HYBRID = 2.02E-14	HYBRID = 1.93E-14	HYBRID = 5.1E-12	HYBRID = 2.1E-14	HYBRID = 2.75E-13
Average error = 1.9E-7	Average error = 3.28E-8	Average error = 3.21E-8	Average error = 5.22E-7	Average error = 3.35E-8	Average error = 1.21E-7
Pb-loaded TDAC					
A_{KC} = 10.098	q_K = 2.296	q_H = 167.23	K_{Js} = 10.437	K_{Fs} = 0.371	K_U = 3.089
B_{KC} = 4.137	a_K = 0.255	K_H = 33.81	a_{Js} = 1.756	q_{Fs} = 13.14	q_U = 8.86
n_{KC} = 1.85	b_K = 1.946	n_H = 0.573	b_{Js} = 0.399	n_{Fs} = 0.622	S_U = 0.016
R^2 = 1	R^2 = 1	R^2 = 1	R^2 = 1	R^2 = 1	R^2 = 1
R^2_{adj} = 1	R^2_{adj} = 1	R^2_{adj} = 1	R^2_{adj} = 1	R^2_{adj} = 1	R^2_{adj} = 1
X^2 = 1.07E-11	X^2 = 4.71E-15	X^2 = 4.19E-12	X^2 = 7.04E-19	X^2 = 8.66E-15	X^2 = 6.33E-14
RMSE = 3.28E-6	RMSE = 6.86E-8	RMSE = 2.04E-6	RMSE = 8.39E-10	RMSE = 9.31E-8	RMSE = 2.51E-7
HYBRID = 2.24E-11	HYBRID = 9.79E-15	HYBRID = 8.73E-12	HYBRID = 1.46E-18	HYBRID = 1.8E-14	HYBRID = 1.32E-13
Average error = 1.09E-6	Average error = 2.29E-8	Average error = 6.83E-7	Average error = 2.8E-10	Average error = 3.1E-8	Average error = 8.39E-8

Holl-Krich	*M-L-F	Langmuir-Jovanovich	Jovanovich-Freundlich	Radke-Praustinz I	Radke-Praustinz II
Cu-loaded TDAC					
K_{HK} = 0.378	K_{mLF} = 2.14	K_{LJ} = -3.10	K_{JF} = 1.00	K_{RI} = 0.353	K_{RII} = 0.360
q_{HK} = 13.11	q_{mLF} = 1.018	q_{LJ} = 12.96	q_{JF} = 1.554	q_{RI} = 13.142	Q_{RII} = 13.14
n_{HK} = 1.90	R^2 = 1	n_{LJ} = 0.554	n_{JF} = 0.366	m_{RI} = 0.673	m_{RII} = 0.636
R^2 = 1	R^2_{adj} = 1	R^2 = 1	R^2 = 1	R^2 = 1	R^2 = 1
R^2_{adj} = 1	X^2 = 1.04E-19	R^2_{adj} = 1	R^2_{adj} = 1	R^2_{adj} = 1	R^2_{adj} = 1
X^2 = 1.78E-13	RMSE = 3.23E-10	X^2 = 5.08E-20	X^2 = 2.5E-13	X^2 = 9.6E-17	X^2 = 1.01E-14
RMSE = 4.22E-7	HYBRID = 2.17E-19	RMSE = 2.25E-10	RMSE = 5.0E-7	RMSE = 9.8E-9	RMSE = 1.01E-7
HYBRID = 3.72E-13	Average error = 1.1E-10	HYBRID = 1.06E-19	HYBRID = 5.2E-13	HYBRID = 2.0E-16	HYBRID = 2.1E-14
Average error = 1.41E-7		Average error = 7.51E-11	Average error = 1.67E-7	Average error = 3.26E-9	Average error = 3.35E-8
Pb-loaded TDAC					
K_{HK} = 0.391	K_{LF} = 2.28	K_{LJ} = -3.19	K_{JF} = 0.99	K_{RI} = 0.359	K_{RII} = 0.371
q_{HK} = 13.13	q_{MLF} = 13.16	q_{LJ} = 12.96	q_{JF} = 1.56	q_{RI} = 13.143	Q_{RII} = 13.141
n_{HK} = 1.899	m_{LF} = 1.005	n_{LJ} = 0.537	n_{JF} = 0.373	m_{RI} = 0.658	m_{RII} = 0.622
R^2 = 1	R^2 = 1	R^2 = 1	R^2 = 1	R^2 = 1	R^2 = 1
R^2_{adj} = 1	R^2_{adj} = 1	R^2_{adj} = 1	R^2_{adj} = 1	R^2_{adj} = 1	R^2_{adj} = 1
X^2 = 3.2E-13	X^2 = 1.06E-19	X^2 = 8.14E-18	X^2 = 9.02E-14	X^2 = 4.38E-15	X^2 = 8.67E-15
RMSE = 5.69E-7	RMSE = 3.25E-10	RMSE = 2.85E-9	RMSE = 3.0E-7	RMSE = 6.62E-8	RMSE = 9.31E-8
HYBRID = 6.73E-13	HYBRID = 2.21E-19	HYBRID = 1.69E-17	HYBRID = 1.88E-13	HYBRID = 9.1E-15	HYBRID = 1.8E-14
Average error = 1.9E-7	Average error = 1.1E-10	Average error = 9.52E-10	Average error = 1.0E-7	Average error = 2.21E-8	Average error = 3.1E-8

*M-L-F Modified Langmuir-Freundlich

Table 4 *continued*

*L-F-J	Marczewko-Jaroniec	Baudu	Fritz-Schlunder IV	Fritz-Schlunder V
Cu-loaded TDAC				
K_{LFJ} = 1.718	m_{MJ} = 0.717	Y_B = -0.288	A = 39.97	K_1 = 1.754
q_{LFJ} = 13.173	K_{MJ} = 0.098	B_B = 1.137	B = 9.086	K_2 = 0.132
n_{LFJ} = 1.013	q_{MJ} = 13.152	q_B = 13.87	a = 1.282	α = 1.116
R^2 = 1	n_{MJ} = 1.243	X_B = 0.209	b = 0.654	β = 0.895
R^2_{adj} = 1	R^2 = 1	R^2 = 1	R^2 = 1	q_{FSV} = 1.240
X^2 = 8.25E-18	R^2_{adj} = 1	R^2_{adj} = 1	R^2_{adj} = 1	R^2 = 1
RMSE = 2.87E-9	X^2 = 3.06E-13	X^2 = 3.13E-12	X^2 = 3.11E-16	R^2_{adj} = 1
HYBRID = 1.72E-17	RMSE = 5.53E-7	RMSE = 1.77E-6	RMSE = 1.77E-8	X^2 = 8.34E-16
Average error = 9.57E-10	HYBRID = 6.36E-13	HYBRID = 6.53E-12	HYBRID = 6.48E-16	RMSE = 5.53E-7
	Average error = 1.84E-7	Average error = 5.9E-7	Average error = 5.88E-9	HYBRID = 1.74E-15
				Average error = 9.62E-9
Pb-loaded TDAC				
K_{LFJ} = 1.720	m_{MJ} = 0.716	Y_B = -0.342	A = 40.70	K_1 = 1.762
q_{LFJ} = 13.168	K_{MJ} = 0.101	B_B = 2.341	B = 9.083	K_2 = 0.127
n_{LFJ} = 1.00	q_{MJ} = 13.152	q_B = 13.825	a = 1.284	α = 1.104
R^2 = 1	n_{MJ} = 1.238	X_B = 0.156	b = 0.653	β = 0.932
R^2_{adj} = 1	R^2 = 1	R^2 = 1	R^2 = 1	q_{FSV} = 1.245
X^2 = 2.41E-23	R^2_{adj} = 1	R^2_{adj} = 1	R^2_{adj} = 1	R^2 = 1
RMSE = 4.91E-12	X^2 = 7.31E-12	X^2 = 5.03E-17	X^2 = 1.60E-16	R^2_{adj} = 1
HYBRID = 5.01E-23	RMSE = 3.0E-7	RMSE = 7.09E-9	RMSE = 1.26E-8	X^2 = 2.54E-15
Average error = 1.64E-12	HYBRID = 1.52E-11	HYBRID = 1.05E-16	HYBRID = 3.33E-16	RMSE = 2.7E-6
	Average error = 9.01E-7	Average error = 2.36E-9	Average error = 4.22E-9	HYBRID = 5.28E-15
				Average error = 1.68E-8

*L-F-J = Langmuir-Freundlich- Jovanovich

3.4. Statistical performance evaluation of predictive adsorption capacity (q_e) for the isotherm models

Statistical analysis using SPSS 13.0 was employed to evaluate the predictive adsorption capacity (q_e) for the studied models. The results of all the significance tests were within a predefined confidence level of 95%. Hence, for this evaluation, the predicted adsorption capacity ($q_{e,\,cal}$) data set (consisting of 5 data points) generated for each model prediction was harmonized based on the number of parameters/predictors in the respective models. For instance, by computing the mean, the $q_{e,\,cal}$ data set obtained for each of the 2-parameter models (see list of models presented in Table 2) will then give rise to a single $q_{e,\,cal}$ data set consisting of 5 data point; thus denoted as distribution B (Table 5). A similar evaluation of mean was conducted for 1-parameter, 3-parameter, 4-parameter and 5-parameter model to generate a single $q_{e,\,cal}$ data set in each case. This single $q_{e,\,cal}$ data set thus generated will be denoted as distribution A (for 1-parameter models), distribution C (for 3-parameter models), distribution D (for 4-parameter models) and distribution E (for 5-parameter models). These distributions (A, B, C, D, and E) were sequentially compared to the experimentally derived adsorption capacity ($q_{e,exp}$, mg/g) to ascertain the influence of the number of parameters in a given model on its $q_{e,\,cal}$ prediction efficiency.

One-sample statistics table which depicts the standard deviation (SD) and standard error mean (SEM) of each distribution for both adsorbents are presented in Table 5. Generally, SD elucidates the closeness of data values to the test mean value. The test means (mean of $q_{e,exp}$ data set) of 9.180 (for Cu-loaded TDAC) and 9.605 (for Pb-loaded TDAC) was employed as an analytical basis. Noteworthy is the fact that the statistical mean value obtained for all distributions (except those of distribution E) for both adsorption systems were relatively equal to the respective test means (mean of $q_{e,exp}$ data set). However, the accruing SD values were not zero, an indication that the individual value that constituted the distributions deviated significantly from the respective test means. In the case of Cu-loaded TDAC (Table 5), distributions C and D depicted SD values of 3.15 and 2.64, respectively; thus suggesting that each value of these distributions was about 3 points away from the test mean. Similarly, the SD values obtained for distributions A, B and E were higher, such that their values deviated from the test mean by about 6.0, 4.0 and 5.0 points, respectively. For Pb-loaded TDAC, the SD values for distributions B (3.20), C (3.16) and D (3.14) were relatively equal, thus implying a deviation of about 3.0. More so, distributions A and E showed a higher variability value of about 5.0 and 4.0, respectively from the test mean. Therefore, based on the statistical mean value, it could be opined that distribution E (corresponding to 5-parameter model data) showed the most variation from the test means value; which is synonymous with poor predictive performance.

Meanwhile, SD was simply applied in the study as descriptive statistics to elucidate the extent of variability between each value of the distributions and the corresponding test means for both adsorbents. To understand the accuracy of the mean of each distribution to the corresponding test means, consideration of the standard error of the mean (SEM) was necessary. Also, the estimation of the reliability of the data sets that gave rise to each distribution (expressed by how close the mean of each distribution is to the test mean), could be realized using SEM. For Cu-loaded TDAC, Table 5 shows the lowest SEM value of 1.18 for distribution D. This implies that with 95% confidence, one could state that the mean of distribution D is about 1.00 SD from the test mean (9.618) since SEM is the SD of the test mean. In the same vein, the SEM value obtained for distributions B, C and E were relatively low. However, the SEM value obtained for distribution A was the largest, about 3.0 SD from the test mean. In the case of Pb-loaded TDAC, similar trends of SEM values were recorded; as the values for distributions B to E were all below 2.0. Therefore, one could opine (with 95 % confidence) that the mean of these distributions was about 2.00 SD from the test mean. Similarly, distribution A gave the largest SEM value of about 2.4 SD of the test mean. Therefore, concerning standard error mean (SEM), the predictive performance for both

adsorption systems could be arranged in descending order as; distribution D > distribution C > distribution B > distribution E > distribution A.

Table 5. One-sample statistics table

	Cu-loaded TDAC				Pb-loaded TDAC			
Distributions	N	Mean	Std. deviation	Std. Error Mean	N	Mean	Std. deviation	Std. Error Mean
A	5	9.6180	5.67087	2.53609	5	9.6046	5.29709	2.36893
B	5	9.6180	3.69289	1.65151	5	9.6046	3.20221	1.43207
C	5	9.6180	3.14925	1.40839	5	9.6546	3.16288	1.41449
D	5	9.6180	2.63770	1.17961	5	9.6046	3.13635	1.40262
E	5	7.8180	4.66893	2.08801	5	8.0046	4.45027	1.89022

To further verify the extent of the statistical variation between the mean of the distributions and the test mean, one-sample t-Test was employed. The nature of the corresponding t-statistic value (t-value) provides useful evidence for possible acceptance or rejection of the specified null hypothesis. A negative t-value implies lower distribution mean in comparison to the test mean, while positive t-value implies the opposite. A negative and positive t-value will provide evidence against the null hypothesis if the alternative hypothesis stated that the distribution mean is less and greater, respectively than the test mean. Similarly, the t-value of zero is an indication that the relationship between the corresponding distribution mean and test mean is exactly captured in the null hypothesis. For this study, the fact that the mean of each of the distributions is equal to the test mean represents the null hypothesis (H_0), while the alternative hypothesis (H_1) states otherwise. The statement of the null and alternative hypothesis could be expressed mathematically as Eqns. 47- 48;

$$H_0: \left(\overline{X_{q_{e,cal}}} = \overline{X_{q_{e,exp}}}\right) \tag{47}$$

$$H_1: \left(\overline{X_{q_{e,cal}}} \neq \overline{X_{q_{e,exp}}}\right) \tag{48}$$

Where; $\overline{X_{q_{e,cal}}}$ is the mean of the respective distributions and $\overline{X_{q_{e,exp}}}$ is the test mean.

For Cu-loaded TDAC, Table 6 shows that the t-value for distributions A, B, C, and D are exactly zero; thus suggesting that the mean of these distributions is exactly equal to the test mean. Also, the negative t-value depicted in the case of distribution E implies that its mean was less than the test mean. Furthermore, the graphical relationship between the distributions and the experimental data is shown in Fig 5(a). From the plot, it was clear that the plotline of all the distributions except distribution E depicted minimal deviation from the experimental curve line. Such observation further corroborates the fact that for Cu-loaded TDAC, single-parameter (expressed as distribution A), 2-parameter (distribution B), 3-parameter (distribution C) and 4-parameter (distribution) model all provided an efficient prediction of the experimental data. A similar observation was made in the case of Pb-loaded TDAC, as Table 7 and Fig 5(b) show that single-parameter (expressed as distribution A), 2-parameter (distribution B), 3-parameter (distribution C) and 4-parameter (distribution) models all provided an efficient prediction of the experimental data.

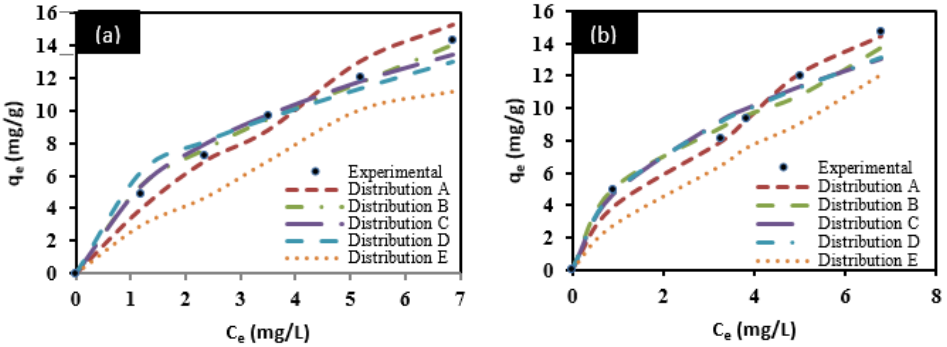

Figure 5. Graphical relationship between the distributions and experimental data sets for (a) Cu-loaded TDAC (b) Pb-loaded TDAC

Just as t-statistics value (t-value) was employed for verifying the extent of the statistical variation between the mean of the distributions and the test mean, the probability value (*p*-value) is useful in determining the statistical significance of a given distribution. It also estimates the probability of observing the expected outcome within the confine of an established null hypothesis. According to Aniagor and Menkiti [1], the lower the *p*-value ($P < 0.05$), the lower the probability of obtaining a similar result as those observed, if the null hypothesis was true. Thus, a lower *p*-value ($P < 0.05$) implies limited support for the established null hypothesis. For Cu-loaded TDAC, the *P*-values for all the distributions (Table 6) was greater than 0.05. But the *P*-values for distributions A, B, C and D were unity and are also numerically larger than that for distribution E. This result shows that although there exists no significant difference between the test mean and those of the various distributions, nevertheless, single-parameter (expressed as distribution A), 2-parameter (distribution B), 3-parameter (distribution C) and 4-parameter (distribution) models provided maximal support for the established null hypothesis; hence portrays higher probability of obtaining a similar result as those observed if the null hypothesis was true. A similar observation was made in the case of Pb-loaded TDAC (Table 7), with all other distributions showing *P*-value equal to unity, except for distribution E (with the lowest p-value of 0.466). This result shows that distribution E (representing the 5-parameter model) offered the lowest probability of obtaining a similar result as those observed if the null hypothesis was true.

Table 6. One-sample t-test table for Cu-loaded TDAC

	Test mean = 9.61801					
	t-value	df	*p*-value	Mean difference	95% Confidence interval of the difference	
Distributions					Lower	Upper
A	.000	4	1.000	0.00000	-7.0413	7.0413
B	.000	4	1.000	0.00000	-4.5853	4.5853
C	.000	4	1.000	0.00000	-3.9103	3.9103
D	.000	4	1.000	0.00000	-3.2751	3.2751
E	-.862	4	0.437	-1.80000	-7.5972	3.9972

Table 7. One-sample t-test table for Pb-loaded TDAC

	Test mean = 9.6046					
	t-value	df	*p*-value	Mean difference	95% Confidence interval of the difference	
Distributions					Lower	Upper
A	.000	4	1.000	.00000	-6.5772	6.5772
B	.000	4	1.000	.00000	-3.9761	3.9761
C	.005	4	0.994	.04999	-3.8773	3.9772
D	.000	4	1.000	.00000	-3.8943	3.8943
E	-.804	4	0.466	-1.60000	-7.1257	3.9257

3.5. Final remark on the statistical evaluation of adsorption capacity (q_e) prediction performance of the isotherm models

Based on t-values and *p*-values, it has been established that the mean $q_{e,\,cal}$ data set of single-parameter (denoted as distribution A), 2-parameter (distribution B), 3-parameter (distribution C) and 4-parameter (distribution D) models were all equal to the test mean (mean of $q_{e,\,exp}$ data set) for the present adsorption system. Hence, one could safely infer that only the 5-parameter model (denoted as distribution E) performed below par in $q_{e,\,cal}$ data prediction for both adsorbents when compared to the other models. Such observation is inconsistent with the literature report by El-Khaiary and Malash [51]. According to the report, an increase in the number of parameter of a given nonlinear model translates to improved and efficient data prediction. However, it has been shown in this study that although the number of the parameter in a given nonlinear model rub off significantly on its $q_{e,\,cal}$ data prediction efficiency, other factors could still influence a given model's data prediction efficiency. Such factors like; the choice of initial parameter guesses during the nonlinear iteration step and prevailing assumption regarding the specified model.

Therefore, for standard deviation (SD) and standard error mean (SEM), distributions A and E provided the poorest predictive performance. However, considering the findings from the statistical mean and one-sample t-test, distribution E depicted the worst predictive performance of all. According to Mario [52], the one-sample t-test is a superior statistical evaluation technique to SEM and SD; thus their result is preferred. Hence, it could be concluded that the experimental equilibrium data obtained for Cu-loaded and Pb-loaded TDAC was well predicted by all the models except the 5-parameter model. This is an indication that irrespective of the number of parameters, a given model can provide an optimum data/parameter prediction provided the choice of initial parameter guess and all other guiding principles/assumptions for the models are carefully considered.

3.6. Evaluation of adsorption potential/density, hopping number and surface coverage.

According to Greenbank and Manes [53], adsorption potential refers to the work done or energy available for the movement of adsorbates from the bulk liquid phase to the adsorbent surface. Often denoted as the negative of the energy of adsorption, it is also a measure of an adsorbates' proximity and subsequent accessibility to a given active site on the adsorbent. Thus, adsorption potential (A) sustains an inverse and direct relationship, respectively with adsorbents pore size and adsorbates ionic radius. An increased adsorption potential implies better adsorption and greater adsorbate packing [53]. Similarly, adsorption density (Γ) refers to the adsorbed (adsorbate) mass per unit adsorbent pore volume. It varies directly with adsorption potential. The relationship between adsorption potential (J/mol) (see Eq. 3), adsorption density (mol/L) (see Eq. 4) and amount of adsorbed heavy metal ions (mg/g) (see Eq. 1) is depicted in Figs. 6 (a-b). The plot showed that these variables vary directly with one another for both adsorption systems. Hence, as the adsorption potential increased, (which implies an increase in energy available for adsorbate transport) corresponding increase in adsorption density (quantity of adsorbate adsorbed

per adsorbent pore volume) was observed. The appreciation of adsorption density with increase in adsorption potential was further corroborated by the observed increment in the amount of adsorbed heavy metal ions [Figs. 6 (a-b)]. Also evident from the plot is the fact that the recorded adsorption density and amount of adsorbed ions for Cu-loaded TDAC system were higher compared to those of Pb-loaded TDAC. This could be because the ionic radius of Cu^{2+} ion (73 picometers [54]) was smaller than that of the Pb^{2+} ion (119 picometers [54]). The implication is that the energy requirement (adsorption potential) for the transport of Cu^{2+} ion from the bulk aqueous phase to the adsorption sites and subsequently into the active sites is minimal when compared to that of Pb^{2+} ion. Therefore, it could be opined that the Cu^{2+} ion (with smaller ionic radius) was readily adsorbed onto the TDAC surface, with denser molecular packing than Pb^{2+} ion. This finding supported the higher removal efficiency recorded for Cu-loaded TDAC adsorption system, as compared to that of Pb-loaded TDAC (see section 3.3).

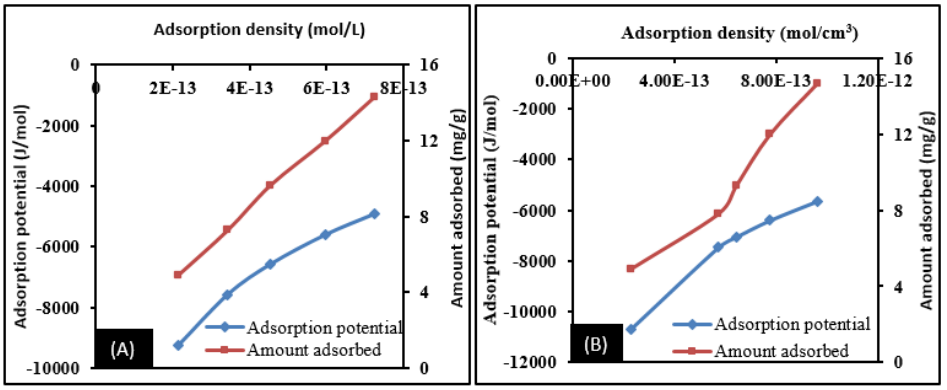

Figure 6. Graphical representation of the relationship between adsorption potential, adsorption density and adsorption capacity for (a) Cu-loaded TDAC (b) Pb-loaded TDAC.

The adsorption behaviour of the present system was further investigated by elucidating the relationship between the hopping number (see Eq. 5), surface coverage (see Eq. 6) and adsorption capacity of the adsorbent (see Eq. 1) as shown graphically in Fig. 7. The plots clearly showed that the adsorption capacity decreased with an increase in hopping number in both Cu-loaded TDAC and Pb-loaded TDAC adsorption systems (Fig. 7). According to Menkiti, et al. [21], a smaller hopping number is synonymous with a faster adsorption process; thus explaining for the observed higher adsorption capacity at a lower hopping number. The plots also showed that with the hopping number, the surface coverage (which is the ratio of the amount of adsorbed substance to the monolayer capacity) sustained an inverse relationship with the adsorption capacity. This is so because even though the migration rate of the adsorbates to potential vacant sites increased with increasing hopping numbers, there would not be much improvement in the monolayer capacity (which could have been saturated at that point) [55]. A critical observation of the plots further showed that the loading of Cu^{2+} ion onto TDAC occurred within a shorter hopping number range when compared to that of Pb^{2+} ion. Therefore, based on the assertion that the smaller hopping number is synonymous with faster adsorption process, one could safely opine that the loading of Cu^{2+} ion onto TDAC occurred faster. This finding corroborates the earlier result obtained in section 3.3, as well as those obtained earlier in section 3.6 (while investigating the adsorption behaviour of our present system to adsorption potential and density).

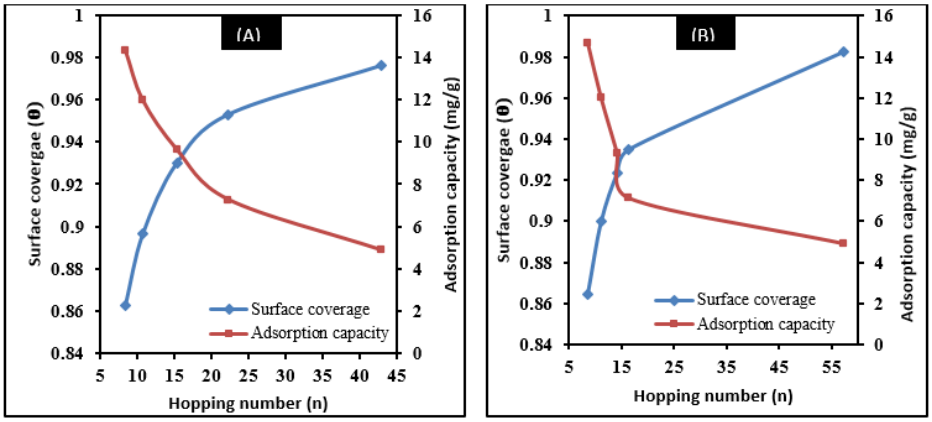

Figure 7. Graphical representation of the relationship between the hopping number, surface coverage and adsorption capacity of the adsorbent for (a) Cu-loaded TDAC (b) Pb-loaded TDAC adsorption system

4. CONCLUSION

- Efficacy of acid-activated carbon (TDAC) sourced from *Gossweilerdendron balsamiferum* (Tola wood) dust (TD) in selected heavy metal (Cu^{2+} and Pb^{2+}) uptake was demonstrated in the present study.
- The optimum pH and contact time recorded in the study were pH 6.0 and 30 min, respectively.
- The FTIR results showed obvious chemical interactions between the adsorbent functional group, as evidenced by the shift and disappearance of several absorption peaks, consequent upon adsorption. Also, the improvement in the surface morphology of the adsorbent due to chemical activation of the precursor was highlighted in the SEM micrograph.
- Analysis of the equilibrium studies of the adsorption system (using the Go-FM models) suggested the best fitting characteristics of the modified Langmuir (ML) model when compared to the other models.
- Statistical evaluation of the predicted data depicted the poor predictive ability of 5-parameter model denoted as distribution E.
- The thermodynamic evaluation of the adsorption potential and adsorption density showed that Cu^{2+} ion was better and readily adsorbed onto TDAC than Pb^{2+} ion.
- The use of TDAC as an adsorbent for selected heavy metal (Cu^{2+} and Pb^{2+} ion) uptake was adjudged effective; with Cu^{2+} depicting better affinity with TDAC.

Declaration of Conflict of Interest

On behalf of all authors, the corresponding author states that there is no conflict of interest concerning this manuscript.

NOMENCLATURE

A	Adsorption Potential (J/mol)
Γ	Adsorption density (mol/cm^3)
r	Ionic radius (cm)
n	Number of data point in a given model
p	Number of the parameter in a given model
RE	Percentage removal (%)
K_H	Henry's adsorption constant
q_{ML}	Maximum adsorption capacity for modified Langmuir model (mg/g)
C_s	Adsorbate saturated concentration (mg/L)
C_e	Equilibrium concentration of adsorbate on adsorbent (mg/L)
K_{ML}	Modified Langmuir constant relating to adsorption capacity (mg/g)
K_F	Freundlich adsorption capacity (L/mg)
n_F	Freundlich constant
R	Universal gas constant (J/K/mol)
T	Absolute temperature (K)
b_T	Tempkin constant relating to the heat of adsorption (J/mol)
K_T	Tempkin isotherm constant (L/g)
K_{Ha} & n_{Ha}	Halsey constant
A_H & B_H	Harkins-Jura constant
q_{mJ}	Maximum adsorption capacity for Jovanovich model (mg/g)
K_J	Jovanovich constant
K_{RP}	Redlich Peterson constant
α_{RP}	Redlich Peterson isotherm constant (L/g)
β_{RP}	Redlich Peterson isotherm exponent
K_S & q_{mS}	Sips isotherm model constant (L/g)
m_s	Sips isotherm exponent
K_{To}, n_{To}, q_{mTo}	Toth isotherm constant (mg/g)
q_{mBS}	Maximum adsorption capacity for Brouer Sotolongo model (mg/g)
K_{BS}	Brouer Sotolongo model constant
α_{BS}	Brouer Sotolongo model parameter relating to adsorption energy
K_{VS}, β_{VS}	Vieth-Sladek model constants
q_{mVS}	Maximum adsorption capacity for Vieth-Sladek model (mg/g)
A_{KC}, B_{KC}, n_{KC}	Koble Corrigans isotherm constants
q_{mK}	Khans isotherm maximum adsorption capacity (mg/g)
b_K	khans isotherm model constant
α_K	khans isotherm model exponent
q_{mHi}, $n_{Hi,}$ K_{Hi}	Hills isotherm constants
K_{Js}, α_{Js}, b_{Js}	Jossens isotherm constants
q_{mFS}	Maximum adsorption capacity for Fritz-Schlunder III (mg/g)
K_{FS}	Fritz-Schlunder III equilibrium constant (mg/g)
n_{FS}	Fritz-Schlunder III model exponent
q_{mU}	Maximum adsorption capacity for Unilan model (mg/g)
K_U	unilan model constant
S	Unilan model exponent
q_{mHK}	Maximum adsorption capacity for Holl-Krich model (mg/g)
K_{HK}	Holl-Krich model parameter
n_{HK}	Holl-Krich isotherm model exponent
K_{MLF}	Modified Langmuir-Freundlich equilibrium constant for heterogeneous solid
m_{MLF}	Modified Langmuir-Freundlich heterogeneous parameter

q_{mLJ} Maximum adsorption capacity for Langmuir-Jovanovich model (mg/g)
K_{LJ} Langmuir-Jovanovich isotherm model constant
n_{LJ} Langmuir-Jovanovich model exponent
q_{mJF} Maximum adsorption capacity for Jovanovich-Freundlich model (mg/g)
K_{JF} Jovanovich-Freundlich isotherm model constant
n_{JF} Jovanovich-Freundlich model exponent
q_{mRI} maximum adsorption capacity for Radke-prausnitz I (mg/g)
K_{RI} Radke-prausnitz I equilibrium constant
m_{RI} Radke-prausnitz I model exponent
q_{mRII} maximum adsorption capacity for Radke-prausnitz-II (mg/g)
K_{RII} Radke-prausnitz II equilibrium constant
m_{RII} Radke-prausnitz II model exponent
q_{mLFJ} Maximum adsorption capacity for Langmuir-Freundlich-Jovanovich (mg/g)
n_{LFJ} Langmuir-Freundlich-Jovanovich model exponent
K_{LFJ} Langmuir-Freundlich-Jovanovich isotherm model constant
q_{mMJ} Maximum adsorption capacity for Marczewki-Jaroniec model (mg/g)
K_{MJ} Marczewki-Jaroniec model constant
n_{MJ} & m_{MJ} Marczewki-Jaroniec parameters characterizing the heterogeneity of an adsorbent surface
q_{mB} Baudu maximum adsorption capacity (mg/g)
b_B Baudu equilibrium constant
x & y Baudu parameter
$A_{FS\ 4}$ & $B_{FS\ 4}$ Fritz-Schlunder IV isotherm model constants
$b_{FS\ 4}$ & $\alpha_{FS\ 4}$ Fritz-Schlunder IV model exponents
$q_{MFS\ 5}$ Maximum adsorption capacity for Fritz-Schlunder V model (mg/g)
K_1, K_2, $\alpha_{FS\ 5}$, $\beta_{FS\ 5}$ Fritz-Schlunder V model parameters

REFERENCES

[1] Aniagor, C.O., Menkiti M.C, Kinetics and mechanistic description of adsorptive uptake of crystal violet dye by lignified elephant grass complexed isolate. Journal of Environmental Chemical Engineering. 2018; 6: 2105–2118. https://doi.org/10.1016/j.jece.2018.01.070

[2] Roger, M.R, Removal of metal ions from contaminated water using agricultural residues. ECO WOOD—2nd International conference on environmentally compatible forest products, 2006; 241–250.

[3] Renge, V.C., Khedkar, S.V., Pande, S.V., Removal of heavy metals from wastewater using low-cost adsorbents: a review. Sci. Rev. Chem. Commun., 2012; 2(4): 580–584.

[4] WHO (World Health Organization). Trace Elements in Human Nutrition and Health, 1996; Geneva, Switzerland.

[5] Menkiti, M.C., Ani, J.U., Onukwuli, O.D., Coagulation flocculation performance of snail shell biomass for wastewater purification. New York Sci. J., 2011; 4(2): 81–90

[6] Menkiti, M.C., Ejimofor, M.I., Ezemagu, I.G., Uddameri, V., Turbid-metric approach on the study of the adsorptive component of paint effluent coagulation using snail shell extract. Arab J. Sci. Eng., 2016; 41: 2527. DOI:10.1007/s13369-015-2013-2

[7] Giri, A.K., Patel, R., Mandal, S, Removal of Cr (VI) from aqueous solution by *Eichhornia crassipes* root biomass-derived activated carbon. Chem. Eng. J., 2012; 34, 185–186

[8] Nethaji, S., Sivasaoyyy, A., Mandal, S, Preparation and characterization of corn cob activated carbon coated with nano-sized magnetite particles for the removal of Cr (VI) Bioresour. Technol., 2013; 134: 94–100.

[9] Saha, B., Orvig, C, Adsorbent for hexavalent chromium elimination from industrial and municipal effluents. Coord. Chem. Rev., 2010; 254: 2959–2972

[10] Albadarin, A.B., Mangwandi, C., Al-Muhtaseb, A.A.H., Walker, G.M. Allen, S.J., Ahmad, M.N.M, Kinetics and thermodynamics of chromium ions adsorption onto low-cost dolomite adsorbent. Chem. Eng. J., 2012; 179: 193–202

[11] Wa Mulange, D.M., Garbers-Craig, A.M, Stabilization of Cr (VI) from fine ferrochrome dust using exfoliated vermiculite. J. Hazard. Mater., 2012; 12: 223–224.

[12] Menkiti M. C., Aniagor C. O, Parametric studies on descriptive isotherms for the uptake of crystal violet dye from aqueous solution onto lignin-rich adsorbent, Arabian Journal of Science and Engineering, 2017; 3(3): 205–220. DOI: 10.1007/s13369-017-2789-3

[13] Yan, H., Yang, H., Li, A.M., Cheng, R.S, pH-tunable surface charge of chitosan/graphene oxide composite adsorbent for efficient removal of multiple pollutants from water. Chem. Eng. J., 2016; 284:1397–1405.

[14] Crini, G., Badot, P.M, Application of Chitosan, a natural Aminopolysaccharide, for dye removal from aqueous solutions by adsorption processes using batch studies: a review of recent literature. Prog. Polym Sci., 2008; 33: 399-447. http://dx.doi.org/10.1016/j.progpolymsci.2007.11.001

[15] *Gupta*, V.K., *Suhas*, Application of Low-Cost Adsorbents for Dye Removal—A Review. Journal of Environmental Management, 2009; 90: 2313-2342.

[16] *Nyiszli, M, Auschwitz: A Doctor's Eyewitness Account. New York: Arcade Publishing, 2011; 34.*

[17] Green, H, Wood: Craft, Culture, History Penguin Books, New York, 2006.

[18] Larous, S.1., Meniai, A.H, Removal of copper (II) from aqueous solution by agricultural by-products sawdust. Energy Procedia, 2012; 18: 915 – 923

[19] Aniagor, C.O, Adsorption of copper (II) and lead (II) metal ions from aqueous solution using Tola (wood) dust activated carbon. Unpublished thesis, Nnamdi Azikiwe University, Awka, 2012.

[20] Horsfall, M., Spiff, A.L, Effects of temperature on the sorption of Pb^{2+} and Cd^{2+} from aqueous solution by *Caladium bicolor* (Wild Cocoyam) biomass. Electronic Journal of Biotechnology, 2005; 8: 2.

[21] Menkiti, M.C., Aneke, M.C., Ejikeme, P.M., Onukwuli, O.D., Menkiti, N.U, Adsorptive treatment of brewery effluent using activated *Chrysophyllum albidium* seed shell carbon. Springerplus, 2014; 3: 213.

[22] Soares, M.A.R., Quina, M.M.J., Gando–Ferreira, L., Quinta–Ferreira, R.M, Removal of Pb (II) from aqueous solutions using eggshell composting products, Second International Conference on Sustainable Solid and Waste Management, Athens, 2014.

[23] Galindo, L.S.G., De, A.F., Neto, A, Removal of cadmium (II) and lead(II) Ions from the aqueous phase on sodic bentonite, Mat. Res., 2013; 16: 515–527.

[24] Menkiti M.C., Aniagor C.O., Agu C.M., Ugonabo V.I, Effective adsorption of crystal violet dye from an aqueous solution using lignin-rich isolate from elephant grass. Water Conservation Science and Engineering, 2018; 3(1): 33 – 46. https://doi.org/10.1007/s41101-017-0040-4

[25] Padmesh, T.V.N., Vijayaraghavan, K., Sekaran, G., Velan, M, Application of two – and three-parameter isotherm models: biosorption of acid red 88 onto *Azolla microphylla*, Biorem. J., 2006; 10: 37–44.

[26] Piccin, J.S., Gomes, C. S., Féris, L.A., Mariliz. G, Kinetics, and isotherms of leather dye adsorption by tannery solid waste. Chemical Engineering Journal, 2012; 183: 30 –38. DOI: 10.1016/j.cej.2011.12.013

[27] Azizian, S., Eris, S., Wilson, L.D, Re-evaluation of the century-old Langmuir isotherm for modeling adsorption phenomena in solution. Chemical physics, 2018; 513: 99-104.

[28] Shafique, U., Ijaz, A., Salman, M., Zaman, W.U., Jamil, N., Rehman, R., Javaid, A, Removal of arsenic from water using pine leaves, J. Taiwan Inst. Chem. E., 2012; 43: 256–263.

[29] Temkin, M.J., Pyzhev V, Kinetics of ammonia synthesis on promoted iron catalysts, Acta Physiochim. URSS, 1940; 12: 217–222.
[30] Foo, K. Y., Hameed, B. H, Insights into the modeling of adsorption isotherm systems, Chemical Engineering Journal, 2010; 156(1): 2–10.
[31] Jovanovic, D.S, Physical sorption of gases: Isotherms for monolayer and multilayer sorption, Colloid Polym. Sci., 1969; 235:1203–1214.
[32] Ng, J.C.Y., Cheung, W.H., McKay, G, Equilibrium studies of the sorption of Cu (II) ions onto chitosan, J. Colloid Interface Sci., 2002; 255: 64–74.
[33] Sips, R, Combined form of Langmuir and Freundlich equations, J. Chem. Phys., 1948; 16: 490 – 495.
[34] Toth, J, State equations of the solid-gas interface layer, Acta Chem. Acad. Hung., 1971; 69: 311 – 317.
[35] Brouers, F., Sotolongo, O., Marquez, F., Pirard, J.P, Microporous and heterogeneous surface adsorption isotherms arising from Levy distributions, Physica A, 2005; 349: 271–282.
[36] Vieth, W.R., Sladek, K.J, A model for diffusion in a glassy polymer, J. Colloid Sci., 1965; 20: 1014–1033.
[37] Hamidpour, M., Kalbasi, M., Afyuni, M., Shariatmadar, H, Kinetic and isothermal studies of cadmium sorption onto bentonite and zeolite, Int. Agrophys., 2010; 24: 253–259.
[38] Khan, A.R., Ataullah, R., Al–Haddad, A, Equilibrium adsorption studies of some aromatic pollutants from dilute aqueous solutions on activated carbon at different temperatures, J. Colloid Interface Sci., 1997; 194: 154–165.
[39] Ringot, D., Lerzy, B., Chaplain, K., Bonhoure, J.P., Auclair, E., Larondelle, Y, In vitro biosorption of ochratoxin A on the yeast industry by-products: comparison of isotherm models, Bioresource Technol., 2007; 98: 1812–1821.
[40] Hadi, M., McKay, G., Samarghandi, M. R., Maleki, A., Aminabad, M.S, Prediction of optimum adsorption isotherm: comparison of chi–square and log–likelihood statistics. Desalination Water Treat., 2012; 49: 81–94.
[41] Fritz, W., Schlunder, E.U, Simultaneous adsorption equilibria of organic solutes in dilute aqueous solution on activated carbon, Chem. Eng. Sci., 1974; 29: 1279–1282.
[42] Shahbeig, H., Bagheri, N., Ghorbanian, S.A., Hallajisani, A., Poorkarimi, S, A new adsorption isotherm model of aqueous solutions on granular activated carbon, WJMS, 2013; 9: 243–254.
[43] Markovski, J.S., Dokic, V., Milosavljevic´, M., Mitric´, M., Peric´–Grujic´, A.A., Onjia, A.E., Marinkovic, A.D, Ultrasonic assisted arsenate adsorption on solvothermal synthesized calcite modified by goethite, α–MnO_2 and goethite/α–MnO_2, Ultrason. Sonochem., 2014; 21: 790–801.
[44] Parker, G.R, Optimum isotherm equation and thermodynamic interpretation for aqueous 1, 1, 2–trichloroethene adsorption isotherms on three adsorbents, Adsorption, 1995; 1: 113–132.
[45] Baudu, M, Etude des interactions solute–fibers de charbon actif. Application et regeneration, Ph.D. diss., Universite de Rennes I, 1990.
[46] Auta, M., Hameed, B.H, Optimized waste tea activated carbon for adsorption of methylene blue and acid blue 29 dyes using response surface methodology. Chem. Eng. J., 2011; 175: 233–243.
[47] Cerozi, B., Fitzsimmons, K. The effect of pH on phosphorus availability and speciation in an aquaponics nutrient solution. Bioresource Technology, 2016; 219: 778–781. 10.1016/j.biortech.2016.08.079.
[48] Delle Site, A. Factors affecting sorption of organic compounds in natural sorbent/ water systems and sorption coefficients for selected pollutants. A review, J. Phys. Chem. Ref. Data, 2001; 30: 187–439.

[49] Jossens, L., Prausnitz, J.M., Fritz, W., Schlünder, E.U., Myers, A.L. Thermodynamics of multi–solute adsorption from dilute aqueous solutions, Chem. Eng. Sci., 1978; 33: 1097–1106.

[50] Quin˜ones, I., Guiochon, G. Derivation and application of a Jovanovic–Freundlich isotherm model for single-component adsorption on heterogeneous surfaces, J. Colloid. Interf. Sci., 1996; 183: 57–67.

[51] El-Khaiary, M.I., Malash, G.F. Common data analysis errors in batch adsorption studies. Hydrometallurgy, 2011; 105(3-4):314–320. https://doi.org/10.1016/j.hydromet.2010.11.005

[52] Mario, F. T. Elementary Statistics, 11TH Ed. Pearson Education Inc. Boston, USA, 2012.

[53] Greenbank, M., Manes, M. Application of the Polanyi Adsorption Potential Theory to Adsorption from Solution on Activated Carbon. J. Phys. Chem., 1981; 85: 3050-3059. Doi: 0022-3654/81/2085-3050$01.25/0

[54] Shannon, R. D. Revised effective ionic radii and systematic studies of interatomic distances in halides and chalcogenides. *Acta Crystallogr. A.*, 1976; 2: 751–767.

[55] McNaught, A. D., Wilkinson, A. IUPAC Compendium of Chemical Terminology, 2nd ed. Blackwell Scientific Publications, Oxford, U.K, 1997.